

Supercritical CO₂-induced atomistic lubrication for water flow in a rough hydrophilic nanochannel

Tuan A. Ho^{1*}, Yifeng Wang², Anastasia Ilgen¹, Louise J. Criscenti¹, and Craig M. Tenney³

¹ *Geochemistry Department, Sandia National Laboratories, Albuquerque, New Mexico 87185, USA.*

² *Nuclear Waste Disposal Research and Analysis Department, Sandia National Laboratories, Albuquerque, New Mexico 87185, USA.*

³ *Nuclear Incident Response Program Department, Sandia National Laboratories, Albuquerque, New Mexico 87185, USA.*

*Corresponding author: taho@sandia.gov

Abstract:

A fluid flow in a nanochannel highly depends on the wettability of the channel surface to the fluid. The permeability of the fluid is usually very low, largely due to the adhesion of fluid at the solid interfaces. Using molecular dynamics (MD) simulations, we demonstrate that the permeability of water in a nanochannel with rough hydrophilic surfaces can be significantly enhanced by the presence of a thin layer of supercritical carbon dioxide (scCO₂) at the water-solid interfaces. The thin scCO₂ layer acts like an atomistic lubricant that transforms a hydrophilic interface into a superhydrophobic one and triggers a transition from a stick- to- a slip boundary condition for a nanoscale flow. This work provides an atomistic insight into multicomponent interactions in nanochannels and illustrates that such interactions can be manipulated, if needed, to increase the throughput and energy efficiency of nanofluidic systems.

Introduction

Fluid slip along a fluid-solid interface is a fundamental topic in nanofluidics.¹⁻³ The degree of fluid slip is quantified by the slip length b , the distance extrapolated from the wall to where the flow velocity equals the wall velocity.⁴ When b is much smaller than the channel height h (i.e., $b \ll h$), the slip can be ignored. This is true for most macroscopic flows for which a no-slip boundary condition is usually applied. Under nanoconfinement, the hydrodynamic slip can no longer be ignored, especially when $b \sim h$.⁴ Large slip length is the main contributor for the massive flow enhancement in carbon nanotubes⁵ and graphene nanopores.^{6,7}

Increasing fluid slip is often assumed to be associated with increasing surface hydrophobicity.⁸⁻¹⁰ However, a few reports have suggested that slip can occur on hydrophilic surfaces^{11, 12} and that water molecules can stick on hydrophobic substrates.¹³ Manipulating surface properties and fluid-surface interactions to obtain a large slip is a matter of growing interest in science and technology, especially for practical applications including self-cleaning surface and energy conversion in nanofluidic devices.¹⁴ Because of the correlation between surface hydrophobicity and hydrodynamic slip, super-hydrophobic surfaces (i.e., with a contact angle larger than 150°) are usually designed to obtain large fluid flow enhancement. Such surfaces can be fabricated by engineering a shear-free air-liquid interface into a solid-liquid one using hydrophobic surface chemistry combining with micro- or nano-scale topological control of the solid surface.^{4, 15, 16}

The question is whether it is possible to obtain a super-hydrophobic surface from an existing hydrophilic one without severely altering its chemistry or physical properties. A transition of a hydrophilic- to a hydrophobic surface may trigger a transformation from a stick- to- a slip boundary condition for a nanoscale flow. Here we present a MD simulation study to demonstrate the possibility for such a transition by exploiting the competitive adsorption of water and scCO₂ onto a rough nanochannel surface. We show that a thin layer of scCO₂ at a water-solid interface can act as an atomistic lubricant that can greatly facilitate a slipping fluid flow in a nanochannel. Our work points to a new mechanism and an engineering approach as well for increasing the throughput and reducing the energy consumption of nanofluidic systems in a wide range of energy-related or other applications.

Results and discussion

The MD simulations were performed on a water-kerogen system in the presence or absence of an accessory fluid or gas (i.e., scCO₂, N₂, or CH₄). Kerogen is a natural carbon material that provides a useful modeling system for understanding a potential effect of surface roughness and functional groups on a fluid flow in nanoconfinement.¹⁷ In addition, kerogen is a major component in a shale gas/oil reservoir, and understanding fluid flows in kerogen nanopores is of great interest to gas/oil production from an unconventional reservoir.¹⁷⁻¹⁹

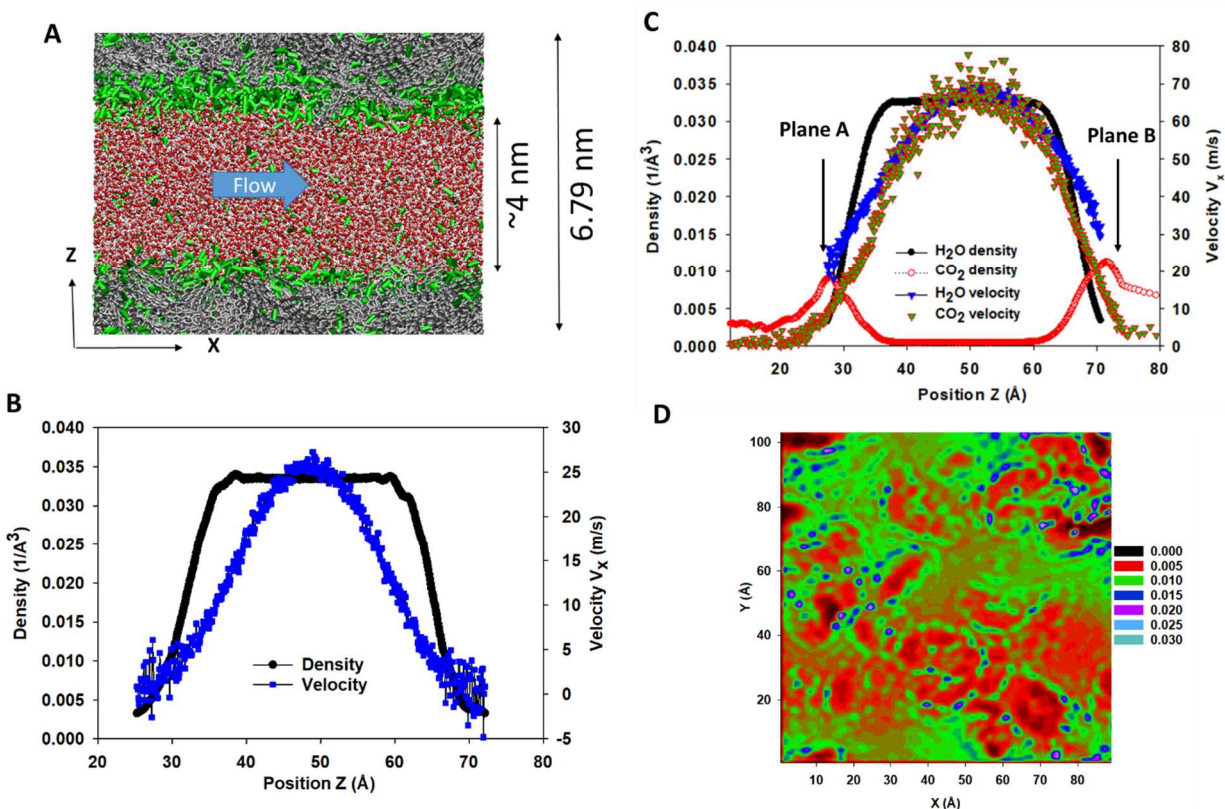


Figure 1. Simulation snapshot illustrating the flow of a water (red and white spheres) and CO₂ (green rods) mixture confined in kerogen nanopore (silver) (A). The size of the system without and with scCO₂ are $8.96 \times 10.36 \times 5.32$ nm³ and $8.96 \times 10.36 \times 6.79$ nm³, respectively. In the flow simulation, water molecules were forced to move in the x direction while the kerogen surface was kept stationary. Density and velocity profiles for pure water (B), and for the water and CO₂ mixture (C) confined in the kerogen nanopore obtained when water flow is fully established. Planes A and B in Fig. C mark top and bottom interfaces. Planar density distribution of CO₂ at top water-CO₂-kerogen interface (D). The color scale in Fig. D represents the density of CO₂ (1/Å³).

In Fig. 1A we present a MD simulation snapshot to illustrate the geometry of a nanochannel used to study fluid flow in kerogen nanopores. It has been documented that significant amounts of water are found in kerogen nanopores, especially fine pores.^{20,21} In this study, we focus on the interaction of multicomponent fluids including CH₄, CO₂, N₂, and H₂O in kerogen nanopores. The kerogen surface in Fig. 1A was created from an over-mature kerogen molecule model shown in Fig. 2A. This realistic kerogen molecule model was designed to represent the chemistry of the kerogen found in the Duvernay shale.²² In our previous work,¹⁷⁻¹⁹ a periodic porous kerogen structure was

built to study both gas adsorption and transport, and the chemo-mechanical coupling between gas sorption and kerogen swelling. In this study, a different approach was employed to build a kerogen surface that is periodic in x and y directions, and non-periodic in z direction. The details of the method and the force field information used for the kerogen surface construction can be found in Supporting Information (SI). To construct the kerogen surface, we first built a kerogen/muscovite interface (Fig. 2B), representing an inorganic/organic interface analogous to those observed in SEM (Scanning Electron Microscope) images of shale samples.²³ The muscovite surface was then removed to create a kerogen-vacuum interface (Fig. 2C). The kerogen surface contains hydrophilic functional groups with oxygen, nitrogen, and sulfur atoms, and hydrophobic hydrocarbon groups as well.²² The result reported in Fig. 2D also suggests that a kerogen surface is rough at an atomistic level. This rough surface is probably a better representation of many actual nanofluidic systems, and the effect of surface roughness on fluid flows is an interesting topic for nanofluidics research.²⁴²⁵ Note that the constrained parameter used to build the kerogen surface is the density of the kerogen slab (see SI for more details). There is no control on the surface roughness in the simulation to construct the kerogen surface.

In our simulations, the water flow was driven in the x direction by an acceleration of 3×10^{-4} Kcal/Å.g (i.e., $\sim 12.55 \times 10^{12}$ m/s²) applied to all water molecules present in the kerogen nanochannel as shown in Fig. 1A (i.e., Poiseuille flow, see SI for more details). The presence or absence of hydrodynamic slip can be studied when a steady state is reached. The temperature was set at 300 K. The pressure in the z direction was 200 atm, which is typical for a shale gas/oil reservoir or geological storage of CO₂. Comparing the velocity profiles of water in the system with and without scCO₂ reveals the effect of scCO₂ on the water flow in kerogen nanochannels. In Fig. 1B, we report the density and velocity profiles of pure water in the kerogen nanopore (i.e., the system without scCO₂). Water-kerogen interface was defined to be the regions where the water density equals 10% of the bulk water density. The density profile indicates that the water density reaches bulk density (~ 0.033 molecules/Å³ or ~ 1 mg/l) at the pore center and gradually reduces toward the kerogen surfaces. Because of the surface roughness, we do not observe multiple interfacial water layers on the kerogen surface as we observe in the 1D density profile for water on a flat surface.¹¹ The velocity profile of water in the nanochannel (Fig. 1B) indicates that at the water-kerogen interface, the water molecules have a zero velocity (with minor fluctuations around

zero due to thermal noises). Therefore, the water flow in the kerogen nanochannel exhibits a no-slip boundary condition.

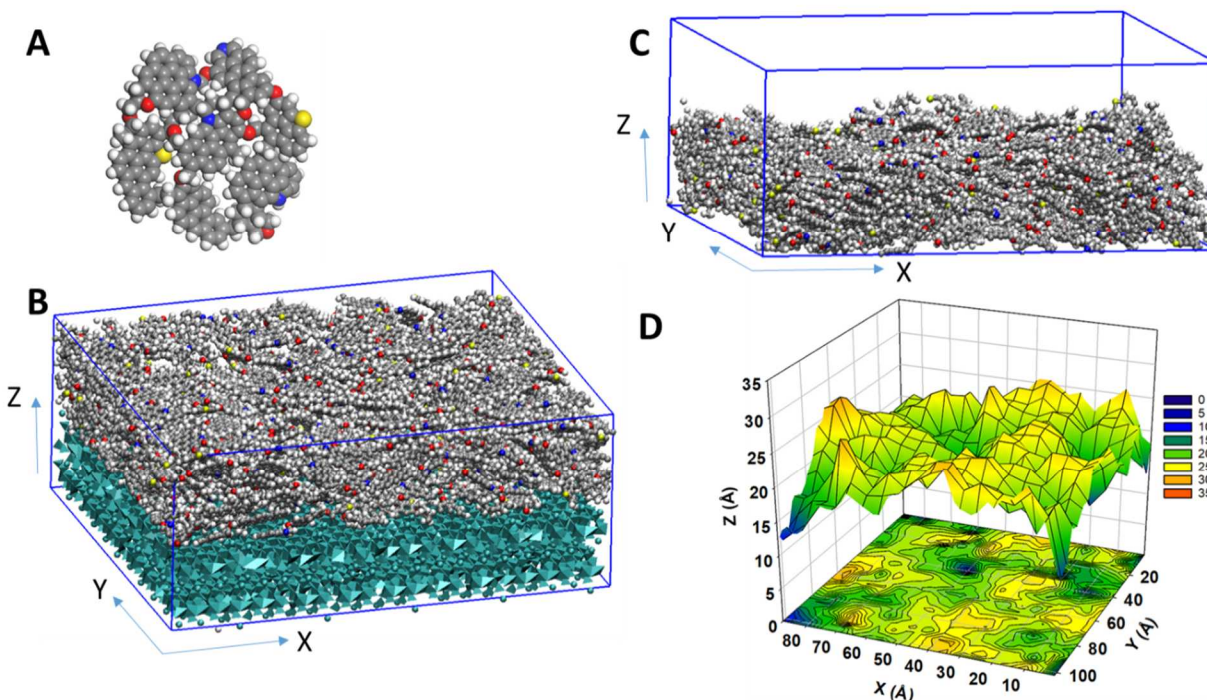


Figure 2. Model kerogen molecule used in this work (A). Note that the color code for kerogen atoms is different from that for kerogen atoms in Fig. 1. Silver, red, blue, yellow, and white spheres represent carbon, oxygen, nitrogen, sulfur, and hydrogen, respectively. Simulation snapshot demonstrates the kerogen/muscovite (cyan) (B) and kerogen/vacuum (C) interfaces. The altitude z of the uppermost kerogen atoms as a function of x and y (D). The contour plot in xy plane is the projection of the z coordinates. The color scale in Fig. D represents the z coordinates.

The no-slip boundary condition observed for water flow in the kerogen nanochannel is consistent with the contact angle result presented in Fig. 3A. A water droplet of 1100 water molecules was placed on the kerogen surface and equilibrated using an NVT ensemble [constant number of atoms, volume, and temperature (300K)]. The contact angle of $42.8^\circ \pm 6.5^\circ$ (see SI for more details about contact angle and error calculations) suggests that a kerogen surface is hydrophilic. Interestingly, when adding scCO_2 at 200 atm into the system of Fig. 3A (see SI) the partially water-wetting kerogen-water interface transforms into a non-water-wetting interface (i.e., with a contact angle of 180° , Fig. 3B). This transition is reversible because when we remove all the CO_2 molecules, the water droplet in Fig. 3B converts back to the droplet in Fig. 3A. The dynamics of the transition

from a small contact angle water droplet into a spherical droplet is of great interest for both fundamental understanding and practical applications, for example, for the development of smart self-cleaning surfaces and more robust coating agents.²⁶ The transition from a hydrophilic to hydrophobic kerogen interface when adding scCO₂ is in good agreement with experimental data that the contact angle of water on mineral surfaces increases with increasing CO₂ pressure.^{27, 28}

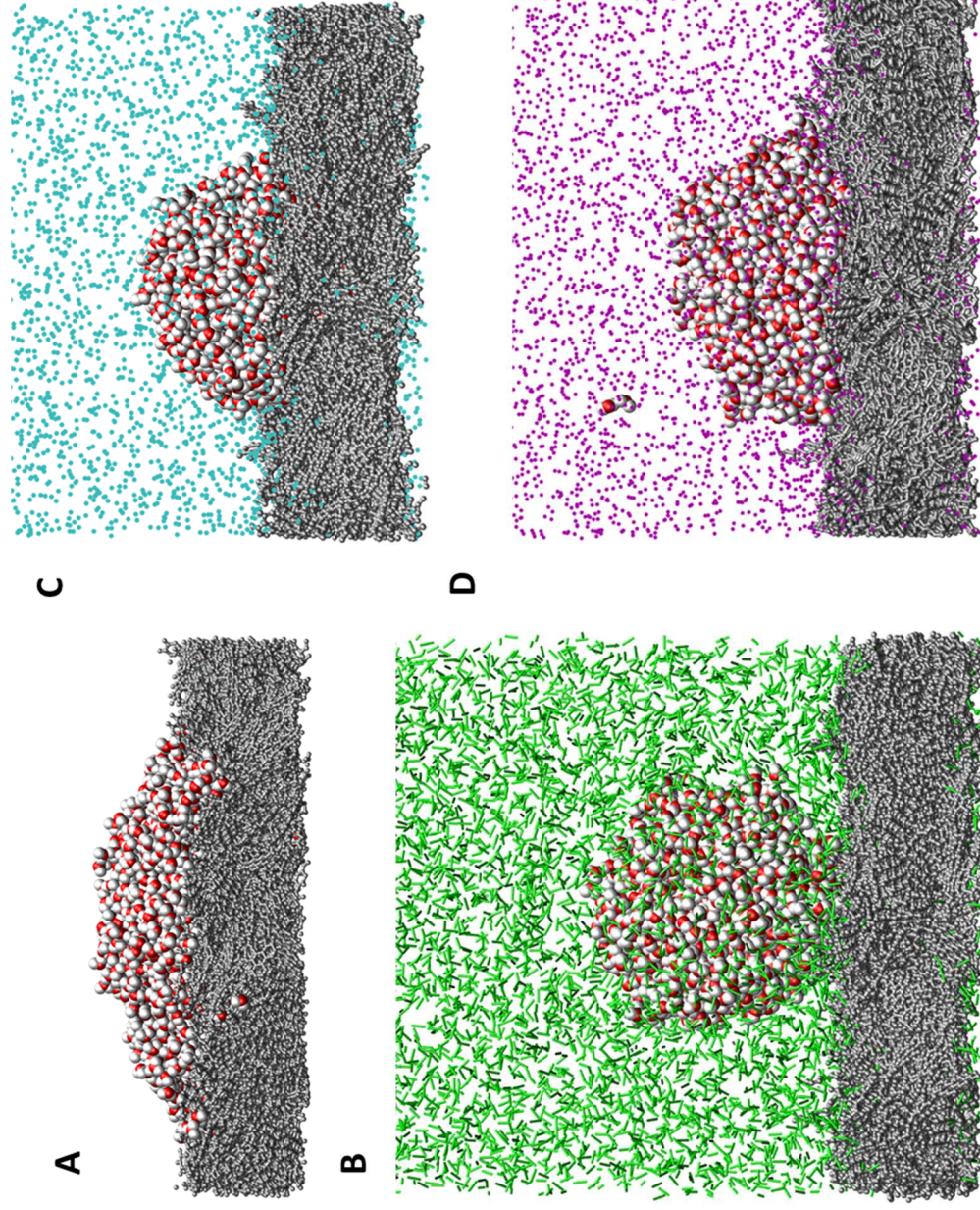


Figure 3. Simulation snapshots illustrating the final configurations of 1100 water molecules droplets in vacuum (A), in 200atm CO₂ (B), N₂ (C), and CH₄ (D) on a kerogen surface. Water molecules are shown in red and white. Kerogen atoms are all colored as silver. CO₂, N₂ and CH₄ are exhibited in green, cyan, and purple, respectively. See SI for force field information and simulation conditions.

When scCO₂ is replaced by N₂ or CH₄ at the same gas pressure (200 atm), the contact angle increases compared to that of water in air (or vacuum). The contact angle of water in 200 atm N₂ (Fig. 3C) or CH₄ (Fig. 3D) is 63.52°±0.21° or 79.18°±1.97°, respectively. However, the contact angle is still smaller than 90°, indicating that the kerogen surface remains hydrophilic in N₂ or CH₄ atmosphere. The competitive adsorption of the scCO₂ over water onto the kerogen surface is the key factor for the transformation of a partially water-wetting into a non-water-wetting interface. In our previous work¹⁹ we show that kerogen has higher affinity for the adsorption of CO₂, compared to CH₄ and N₂. For this reason, the contact angle of water droplet in scCO₂ is larger than that of water droplet in CH₄ and N₂ at the same gas pressure.

The dewetting of a small contact angle droplet into a spherical drop by adding scCO₂ presented in Fig. 3 has interesting consequence regarding the water flow in nanochannel. In Fig. 1C, we show both water and scCO₂ densities and velocities within the kerogen nanochannel. The water concentration is the same as in Fig. 1B. The CO₂ molecules were introduced in the middle of the pore (see SI) at the beginning of the simulation with a CO₂/water ratio of ~0.19 (2100 CO₂ and 10950 H₂O molecules). The pressure and temperature are the same as those used for the system in Fig. 1B (T = 300 K, P = 200 atm). At equilibrium, some CO₂ molecules adsorb inside the kerogen structure, and some CO₂ molecules dissolve into the water. However, the focus of this discussion is the CO₂ layer formed at the water-kerogen interface (i.e., 10Å CO₂ layers centered at planes A and B in the density profile in Fig. 1C, more details of the configuration of the CO₂ layer with respect to kerogen atoms is provided in the SI). These CO₂ layers form because of the competitive adsorption of CO₂ over H₂O onto kerogen surfaces, which will be explained later.

The velocity profile of CO₂ indicates that CO₂ flow exhibits a no-slip boundary condition at kerogen/CO₂ interface. At CO₂/water interface, water flows faster than CO₂ (i.e., at planes A and B in Fig. 1C, note that there is no external force applied on CO₂ molecules, CO₂ molecules move in the x direction is because of the interaction with water). Therefore, water slips on CO₂ layers. The velocities of water at planes A and B in Fig. 1C are 22 m/s and 32 m/s, respectively. From the slip velocity one can estimate the friction coefficient λ using $\lambda = \frac{F_f}{2Av_s}$ where F_f is the friction force (force parallel to the flow direction), v_s is the slip velocity, A is the surface area, and factor '2' is for two interfaces in our simulation box.^{3, 29, 30} The friction force equals the total external force acting on all water molecules (i.e., 59.13 Kcal/mol.Å). For the flow with CO₂ layers, the friction

coefficients are $\sim 100 \times 10^4$ and $\sim 69 \times 10^4$ Ns/m³ at planes A and B, respectively. For the case of no-slip boundary condition of water flow without CO₂, (i.e., zero slip velocity $v_s=0$) one can estimate the friction coefficient from the equilibrium data (i.e., obtained from equilibrium simulation without external force) using the Green-Kubo relation, which is beyond the scope of this work.³
³¹ In addition, the calculated slip lengths at planes A and B are $8.56 \pm 1.00 \text{ \AA}$ and $15.81 \pm 4.28 \text{ \AA}$, respectively (see SI for more details). The differences in the slip velocity and slip length at planes A and B are due to the fact that the kerogen interfaces at planes A and B are not the same and the amount of CO₂ accumulated at planes A and B is different (see the CO₂ density profile). The finite velocities at planes A and B strongly indicate that water flow in the kerogen nanochannel in the presence of scCO₂ exhibits hydrodynamic slip, which is substantially different from the no-slip water flow observed in Fig. 1B.

Because of the slip effect the water flow rate for the system with scCO₂ is ~ 4 times higher than that for the system without scCO₂ (i.e., enhancement factor of 4, comparing on the basis of the same amount of water molecules in the kerogen nanochannel). The result thus demonstrates the capability of an interfacial scCO₂ layer acting as an atomistic lubricant in enhancing water flow in a nanochannel with rough hydrophilic surfaces. This idea is in some sense similar to the existing approach to engineering a shear-free air-liquid interface into a solid-liquid interface by introducing nanometer to micrometer-scale roughness onto a solid surface,³² but here a gas-liquid interface is introduced at a much smaller scale (at a molecular scale). We believe that surface roughness is not necessary for the enhanced permeability. The preferential adsorption of scCO₂ over water onto a smooth surface would enhance the flow rate of water as well. In Fig. 1D we show the surface density distribution of scCO₂ on the xy plane (i.e., density map). The CO₂ molecules within the 10 Å layer centered at the plane B were considered in this calculation. The density map indicates that CO₂ molecules spread all over the kerogen surfaces; however, the molecules are not evenly distributed because of the surface roughness. This illustrates the effectiveness of scCO₂ to intercalate between water and kerogen surfaces to form a new kerogen-scCO₂-water interface.

In our work, the simulation box is periodic in the flow direction. Some CO₂ molecules in the middle of the pore and in the layers at planes A and B leave the channel at one end and enter the channel at the other end (see CO₂ velocity profile in Fig. 1C). The CO₂ density profile indicates that CO₂ layers remain in between water and kerogen during flow simulation. In reality, the

channel is usually short and has two ends. To maintain the lubricant effect for water flow, we may need to introduce additional CO₂ with water at the entrance.

To provide more details about (1) the competitive adsorption of CO₂ over H₂O onto a kerogen surface leading to the formation of a stable CO₂ layer between H₂O and kerogen as shown in Fig. 1 and (2) the larger contact angle of water droplet in CO₂ environment compared to that of water droplet in CH₄ atmosphere shown in Fig. 3, we conducted additional simulations to analyze the interaction energy of CO₂, CH₄, and H₂O with kerogen. In these simulations 2462 of pure CO₂, CH₄, or H₂O molecules were placed in the simulation box of 89.67x103.66x100 Å³ with a kerogen surface present. The simulations were carried out for 3ns in the NVT ensemble. The total pair interaction energy (i.e., that of 2462 molecules with kerogen including the Lennard-Jones (LJ) and electrostatic (Coulomb) interactions) reported in Fig. 4A indicates that CO₂ interacts with kerogen stronger, compared to H₂O. The interaction of CO₂ with kerogen was decomposed into the LJ and electrostatic interactions (Fig. 4B, red and blue lines), and the result suggests that the LJ interaction is much larger than the electrostatic interaction. Further analysis of the LJ interaction of CO₂ with kerogen indicates that LJ interaction from 2 oxygen atoms of CO₂ with kerogen (Fig. 4B, purple line) plays an important role in the CO₂ interaction with kerogen surface. Similarly, for water (Fig.4C), the LJ interaction with kerogen is stronger than the electrostatic interaction. Note that the electrostatic interaction of water with kerogen is stronger compared to that of CO₂ with kerogen (red lines in Fig. 4B and 4C), which is expected due to the strong dipole moment of water compared to the zero external dipole moment of CO₂.^{28, 33} However, the LJ interaction of CO₂ with kerogen is sufficiently strong, compared to that of water leading to formation of stable CO₂ layers between kerogen and H₂O. In addition, the molecular model of kerogen presented in Fig. 2A indicates that the over mature kerogen is composed of large segments of the aromatic hydrocarbons, which is similar to the structure of graphene. On the perfect graphene surface the selectivity of CO₂ over water is ~7.2.³³

The comparison of the interaction energy of CO₂ and CH₄ with kerogen presented in Fig. 4A explains the larger contact angle of water on kerogen surface in CO₂ atmosphere, compared to that of water on kerogen surface in CH₄ atmosphere (as presented in Fig 3). Contact angle θ of water can be calculated using Young's equation:

$$\cos\theta = \frac{\gamma_{s/g} - \gamma_{s/w}}{\gamma_{g/w}} \quad (1)$$

Where γ is the surface tension and s , g , and w are for solid, gas, and water, respectively. Our results indicate that contact angle of water in CO₂ is greater than that of water in CH₄ environment:

$$\cos\theta_{w/\text{CO}_2} < \cos\theta_{w/\text{CH}_4} \quad (2)$$

Combining (1) and (2) we have

$$\frac{\gamma_{s/\text{CO}_2} - \gamma_{s/w}}{\gamma_{\text{CO}_2/w}} < \frac{\gamma_{s/\text{CH}_4} - \gamma_{s/w}}{\gamma_{\text{CH}_4/w}} \quad (3)$$

In our simulation, solid phase (i.e., kerogen) and water are the same in CO₂ and CH₄ environments, therefore $\gamma_{s/w}$ is constant. Because $\gamma_{\text{CO}_2/w} < \gamma_{\text{CH}_4/w}$ ³⁴⁻³⁶ inequality (3) is true when $\gamma_{s/\text{CO}_2} \ll \gamma_{s/\text{CH}_4}$. To the best of our knowledge, there is no reported interfacial tension of kerogen with CO₂ and CH₄ available in the literature. However, the comparison of the interaction energy of CO₂ and CH₄ with kerogen reported in Fig. 4A indicates that CO₂ interacts more strongly with kerogen compared to CH₄. In addition, in our previous work¹⁹ kerogen preferentially adsorbs CO₂ over CH₄. Therefore, we postulate that $\gamma_{s/\text{CO}_2} \ll \gamma_{s/\text{CH}_4}$.

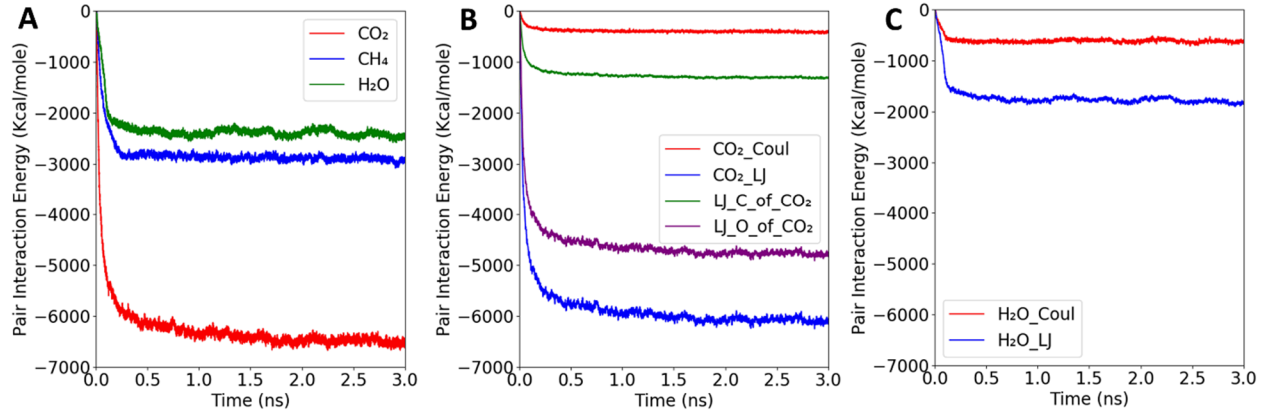


Figure 4. Pair interaction energy of CO₂ (red), CH₄ (blue), and H₂O (green) molecules with kerogen (A). Electrostatic (red) and LJ (blue) interactions of CO₂ molecules with kerogen, and the LJ interactions of the carbon (green) and oxygen (purple) atoms of CO₂ molecule with kerogen (B). Electrostatic (red) and LJ (blue) interaction energy of water with kerogen (C).

Recent experimental and modeling studies have illustrated that with decreasing nanopore size, the thermodynamic properties of water are altered. A decrease in the dielectric constant by 50% was

reported for 1.2 nm pore.^{37, 38} A decrease in density and surface tension was also reported for confined water, compared to the bulk phase.³⁹ These changes in water properties are due to the distortion in hydrogen-bonding networks, with increasing hydrogen-bonding and increasing fraction of 4-coordinated waters with decreasing pore size.^{40, 41} The pore diameter modeled in our study was ~4 nm, which is at the scale where a nanoconfinement effect may become pronounced. Given the earlier observations and our results, we hypothesize that with decreasing pore size and decreasing water density, the effect of the atomistic lubricant will be increasing. We do not anticipate any significant nanoconfinement effect for scCO₂, in comparison to H₂O, since CO₂ molecules lack dipole moment.

The wettability of kerogen under the different conditions presented in Fig. 3 is critical for understanding the fate of aqueous hydraulic fracturing fluids, CO₂, and CH₄ in shale reservoirs and in shale caprock during geological carbon storage.⁴² Traditional wisdom is that the shale organic pore is hydrophobic.⁴² However, our results show that kerogen is partially water-wetting (Fig. 3A, C, and D) due to its hydrophilic functional groups and surface roughness. This conclusion is consistent with the fact that water has been experimentally found in organic nanopores, especially with decreasing pore size.^{20, 21} In addition, the result shown in Fig. 3B indicates that kerogen is CO₂-wetting and that CO₂ can expel water from kerogen interfaces. These conclusions together with our previous result show that CO₂ can displace large amount of CH₄ in kerogen nanopores¹⁹ indicate that kerogen could provide an effective sink for CO₂ during geological storage. We also want to postulate that the lubrication mechanism demonstrated above may have an implication to the release of produced water in an unconventional oil/gas reservoir, an interesting topic certainly worth further research. In addition, a large contact angle of water droplet in scCO₂ environment was also observed on siloxane surface of kaolinite, and a CO₂ layer was also found between kaolinite and water droplet.⁴³ This can serve as an indirect piece of evidence that CO₂ can sandwich not only between kerogen and water, but also between mineral and water.

Conclusions

In summary, using molecular dynamics simulations of water flow in a realistic kerogen nanochannel, we have demonstrated that a stick to slip transition of a water flow in a nanochannel can be induced by incorporating an accessory fluid component (e.g., scCO₂), which has a limited solubility in water and, through competitive adsorption, can spontaneously form an atomistically

thin layer over a rough hydrophilic surface and therefore lubricate the water in the nanochannel. Once verified experimentally, this result can provide a new engineering approach to obtain a hydrophobic or super-hydrophobic interface from an existing hydrophilic one without significantly alteration in surface topology. This could lead to the technological advancement for a variety of applications including water desalination and energy conversion in nanofluidic devices.

Conflicts of interest

There are no conflicts to declare.

Acknowledgements

Sandia National Laboratories is a multi-mission laboratory managed and operated by National Technology and Engineering Solutions of Sandia, LLC., a wholly owned subsidiary of Honeywell International, Inc., for the U.S. Department of Energy's National Nuclear Security Administration under contract DE-NA0003525. The views expressed in this article do not necessarily represent the views of the U.S. Department of Energy or the United States Government. This research was funded by a DOE National Energy Technology Laboratory project (to Y. Wang) and by the Center for Frontiers in Subsurface Energy Security, an Energy Frontier Research Center funded by the U.S. Department of Energy, Office of Science, Office of Basic Energy Sciences under Award Number DE-SC0001114.

References

1. I. U. Vakarelski, E. Klaseboer, A. Jetly, M. M. Mansoor, A. A. Aguirre-Pablo, D. Y. C. Chan and S. T. Thoroddsen, *Sci Adv*, 2017, **3**, e1701558.
2. J. C. T. Eijkel and A. van den Berg, *Microfluid. Nanofluid.*, 2005, **1**, 249-267.
3. G. Tocci, L. Joly and A. Michaelides, *Nano Lett.*, 2014, **14**, 6872-6877.
4. R. S. Voronov, D. V. Papavassiliou and L. L. Lee, *Ind Eng Chem Res*, 2008, **47**, 2455-2477.
5. J. K. Holt, H. G. Park, Y. M. Wang, M. Stadermann, A. B. Artyukhin, C. P. Grigoropoulos, A. Noy and O. Bakajin, *Science*, 2006, **312**, 1034-1037.
6. B. Radha, A. Esfandiari, F. C. Wang, A. P. Rooney, K. Gopinadhan, A. Keerthi, A. Mishchenko, A. Janardanan, P. Blake, L. Fumagalli, M. Lozada-Hidalgo, S. Garaj, S. J. Haigh, I. V. Grigorieva, H. A. Wu and A. K. Geim, *Nature*, 2016, **538**, 222-225.
7. R. R. Nair, H. A. Wu, P. N. Jayaram, I. V. Grigorieva and A. K. Geim, *Science*, 2012, **335**, 442-444.
8. D. Ortiz-Young, H. C. Chiu, S. Kim, K. Voitchovsky and E. Riedo, *Nat Commun*, 2013, **4**, 2482
9. K. L. Wu, Z. X. Chen, J. Li, X. F. Li, J. Z. Xu and X. H. Dong, *Proc. Natl. Acad. Sci. U.S.A.*, 2017, **114**, 3358-3363.
10. D. M. Huang, C. Sendner, D. Horinek, R. R. Netz and L. Bocquet, *Phys. Rev. Lett.*, 2008, **101**, 226101
11. T. A. Ho, D. V. Papavassiliou, L. L. Lee and A. Striolo, *Proc. Natl. Acad. Sci. U.S.A.*, 2011, **108**, 16170-16175.

12. K. P. Lee, H. Leese and D. Mattia, *Nanoscale*, 2012, **4**, 2621-2627.
13. C. Bakli and S. Chakraborty, *Nano Lett.*, 2015, **15**, 7497-7502.
14. D. Gillespie, *Nano Lett.*, 2012, **12**, 1410-1416.
15. H. B. Hu, J. Wen, L. Y. Bao, L. B. Jia, D. Song, B. W. Song, G. Pan, M. Scaraggi, D. Dini, Q. J. Xue and F. Zhou, *Sci Adv*, 2017, **3**, e1603288.
16. J. P. Rothstein, *Annu Rev Fluid Mech*, 2010, **42**, 89-109.
17. T. A. Ho, L. J. Criscenti and Y. F. Wang, *Sci. Rep.*, 2016, **6**, 28053.
18. T. A. Ho, Y. Wang and L. J. Criscenti, *Phys. Chem. Chem. Phys.*, 2018, **20**, 12390-12395.
19. T. A. Ho, Y. Wang, Y. Xiong and L. J. Criscenti, *Fuel*, 2018, **220**, 1-7.
20. X. Gu, D. F. R. Mildner, D. R. Cole, G. Rother, R. Slingerland and S. L. Brantley, *Energy Fuel*, 2016, **30**, 4438-4449.
21. L. F. Ruppert, R. Sakurovs, T. P. Blach, L. L. He, Y. B. Melnichenko, D. F. R. Mildner and L. Alcantar-Lopez, *Energy Fuel*, 2013, **27**, 772-779.
22. P. Ungerer, J. Collell and M. Yiannourakou, *Energy Fuel*, 2015, **29**, 91-105.
23. F. P. Wang and R. M. Reed, *SPE*, 2009, **124253**.
24. R. Qiao, *Microfluid. Nanofluid.*, 2007, **3**, 33-38.
25. A. Q. Shen, Y. K. Liu, X. H. Qiu, Y. J. Lu and S. Liang, *Appl. Phys. Lett.*, 2017, **110**, 121601
26. A. M. J. Edwards, R. Ledesma-Aguilar, M. I. Newton, C. V. Brown and G. McHale, *Sci Adv*, 2016, **2**, e1600183.
27. P. Chiquet, D. Broseta and S. Thibeau, *Geofluids*, 2007, **7**, 112-122.
28. S. Iglauer, *Acc. Chem. Res.*, 2017, **50**, 1134-1142.
29. S. Nakaoka, Y. Yamaguchi, T. Omori, M. Kagawa, T. Nakajima and H. Fujimura, *Phys. Rev. E*, 2015, **92**.
30. C. L. Wang, B. H. Wen, Y. S. Tu, R. Z. Wan and H. P. Fang, *J. Phys. Chem. C*, 2015, **119**, 11679-11684.
31. L. Bocquet and J. L. Barrat, *Phys. Rev. E*, 1994, **49**, 3079-3092.
32. A. B. D. Cassie and S. Baxter, *Trans. Faraday Society*, 1944, **40**, 0546-0550.
33. Y. Y. Liu and J. Wilcox, *Environ. Sci. Technol.*, 2013, **47**, 95-101.
34. Q. Y. Ren, G. J. Chen, W. Yan and T. M. Guo, *J. Chem. Eng. Data*, 2000, **45**, 610-612.
35. S. Khosharay and F. Varaminian, *Int J Refrig*, 2014, **47**, 26-35.
36. Y. L. Liu, H. A. Li and R. Okuno, *Ind Eng Chem Res*, 2016, **55**, 12358-12375.
37. J. Marti, G. Nagy, E. Guardia and M. C. Gordillo, *J. Phys. Chem. B*, 2006, **110**, 23987-23994.
38. S. Senapati and A. Chandra, *J. Phys. Chem. B*, 2001, **105**, 5106-5109.
39. T. Takei, K. Mukasa, M. Kofuji, M. Fuji, T. Watanabe, M. Chikazawa and T. Kanazawa, *Colloid Polym Sci*, 2000, **278**, 475-480.
40. S. Le Caer, S. Pin, S. Esnouf, Q. Raffy, J. P. Renault, J. B. Brubach, G. Creff and P. Roy, *Phys. Chem. Chem. Phys.*, 2011, **13**, 17658-17666.
41. X. F. Huang, Q. Wang, X. X. Liu, S. H. Yang, C. X. Li, G. Sun, L. Q. Pan and K. Q. Lu, *J. Phys. Chem. C*, 2009, **113**, 18768-18771.
42. Y. Hu, D. Devegowda, A. Striolo, A. Phan, T. A. Ho, F. Civan and R. F. Sigal, 2014, **20**, SPE-167234-PA.
43. C. M. Tenney and R. T. Cygan, *Environ. Sci. Technol.*, 2014, **48**, 2035-2042.